Compact CPW-fed Antenna with Controllable WLAN Band-rejection for Microwave Imaging

Mokhtar Mokhtari[1,2], Rachid Oussaid[1], Ali Mansoul[2] and Mouloud Challal[3]

[1] Laboratory of Instrumentation (LINS), Faculty of Electrical Engineering, University of Sciences and Technology Houari Boumediene (USTHB), Bab Ezzouar, Algeria

[2] Center for Development of Advanced Technologies, Baba Hassen, Algeria

[3] Institute of Electrical and Electronic Engineering, University M'Hamed BOUGARA of Boumerdes, Boumerdes, Algeria

Corresponding author: Mokhtar Mokhtari (e-mail: m.mokhtari.1@hotmail.com).

ABSTRACT This work presents the design and experimental validation of a compact frequency-reconfigurable coplanar waveguide (CPW)-fed ultra-wideband (UWB) antenna for application in microwave imaging systems with a capability to switch between UWB modes, with and without WLAN band-notched features. The suggested topology and design process are used to achieve an enhancement in the bandwidth using T-shaped slots between the feedline and the ground plane of the antenna, whereas the WLAN band is rejected using an open loop resonator (OLR) placed on the antenna backside. Switching between UWB with and without WLAN band-notched modes is performed using a single PIN diode. The simulation results corroborate well with the experimental data and clearly show an interesting frequency reconfigurable behavior for use in microwave imaging applications. The antenna performance simulation and analysis model is presented for breast tumor detection.

INDEX TERMS Reconfigurable antenna, Microwave imaging, Band-notched, PIN diode.

I. INTRODUCTION

Microwave imaging has emerged as a promising tool in the field of medical diagnostics, particularly in the context of breast cancer detection. This modality exploits disparities in dielectric properties between healthy and malignant tissues. In comparison to established imaging techniques such as magnetic resonance imaging and X-ray mammography, microwave imaging offers advantages in terms of cost-effectiveness and the utilization of non-ionizing radiation [1].

For effective implementation of microwave imaging, ultra-wideband (UWB) antennas are indispensable due to their capability to generate short pulses in the time domain, facilitating high data rates [2]. Furthermore, the flexibility of UWB antennas allows for the combination of low frequencies, enabling enhanced penetration depth, and high frequencies, contributing to superior image resolution [3]. A comparative study of antennas for microwave imaging systems, as presented in [4], shows that the gain varies from 2.43 dBi to 8.4 dBi depending on the antenna characteristics. Increasing the antenna size leads to increased gain; however, there is a trade-off between achieving acceptable gain and managing the antenna size.

Numerous UWB antennas have been proposed for microwave imaging applications, encompassing diverse designs such as square microstrip monopole antennas [5], CPW taper arc slot antennas [6], flexible dual-polarized antennas [7], hibiscus petal pattern-shaped antennas [8], slotted patch antennas [2,9,10], and vivaldi antennas [11,12]. On the other hand, to avoid potential interference between UWB and other communication standards, deploying UWB antennas featuring band-notch characteristics has been suggested for microwave imaging. In [13], a UWB antenna incorporating a semi-elliptical defected ground structure, and featuring an X-band notch using a C-structured reflector has been reported. Furthermore, in [14], a UWB polygon antenna with WiMAX and WLAN bands notched has been proposed; the band-rejections were obtained using ring slot and EBG structures. Moreover, [15] described a monopole antenna featuring double U-shaped slots on the radiating element to reject WLAN and WiMAX bands. Additionally, in [16], a Multiple Input Multiple Output (MIMO) UWB slot antenna with WLAN band-notched using U-shaped slot has also been presented.

The concept of frequency reconfigurable antennas (FRA) offers the advantage of integrating various operating modes, such as narrowband, multi-band, UWB, and band-notch, within a single antenna. The transition between these operating modes can be achieved through mechanisms like Micro-Electro-Mechanical Systems (MEMS) [17], varactor diodes [18], or PIN diodes [19, 20]. Whereas FRAs find widespread use in emerging communication standards [20, 21], their application in microwave imaging systems has been relatively limited. In the literature, a CPW antenna with a tunability feature using varactors [22] has been

reported, as well as a tapered slot antenna that switches between UWB and narrowband modes [23].

This paper introduces a compact coplanar waveguide (CPW)-fed antenna with a capability to switch between UWB modes, with and without WLAN band-notched features, specifically designed for microwave imaging applications. The antenna design and simulation are conducted using CST Microwave Studio, comprising a square radiating patch fed by a 50-ohm CPW line, T-shaped slots, and an open-loop resonator (OLR). The novel design strategies involve using a single OLR on the antenna backside to create a band-notch and employing a single PIN diode to achieve a straightforward frequency-reconfigurable antenna with a simple switching mechanism. Additionally, the antenna is proposed for application in microwave imaging systems, operating in both interfered and uninterfered environments.

II. ANTENNA DESIGN

A. DESIGN OF UWB ANTENNA

The geometric layout of the initial UWB antenna is shown in Fig. 1(a). The antenna is printed on an FR4 substrate of 1.6 mm in thickness, a relative permittivity of 4.3, and a loss tangent of 0.025. The proposed antenna consists of a square radiating patch fed by a 50 Ohm CPW line, a pair of T-shaped slots is introduced into the ground plane to create a new resonance at 9.2 GHz and allow the bandwidth to be increased from [2.94-8.75 GHz] to [2.94-11 GHz], it signifies an improvement of 16.23 % in bandwidth and covers the entire UWB band. T-shaped slots influence the surface current distribution along both X and Y axes, whereas the vertical (or the horizontal) rectangular slot affects only one axis. The optimized antenna dimensions are listed in Table I.

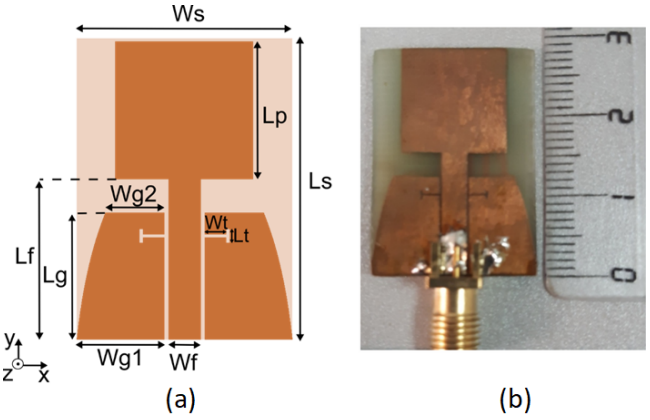

FIGURE 1. Proposed UWB antenna. (a) Layout and, (b) Fabricated prototype.

TABLE I. Physical dimensions of the UWB antenna

Parameter	Value (mm)	Parameter	Value (mm)
Ws	20	*Ls*	28
Wf	3	*Lf*	14.9
Wg1	8.14	*Lg*	11.8
Wg2	5.47	*Lp*	12.8
Wt	2	*Lt*	1.3

In order to ensure that the proposed antenna performance could meet the desired bands, parametric studies are carried out. The effect of varying the length of the radiating element "Lp", and the ground plane length "Lg" are investigated as shown in Fig. 2. It is clearly demonstrated that the "Lp" value influences significantly on the first resonant frequency. Increasing the length of "Lp" results in a downward shift of the lower edge frequency, while decreasing the length has the opposite effect. Additionally, the "Lg" affects the impedance matching of the antenna. Interesting results were obtained with Lg = 11.8 mm, which allows a better coupling between the ground plane and the radiating element.

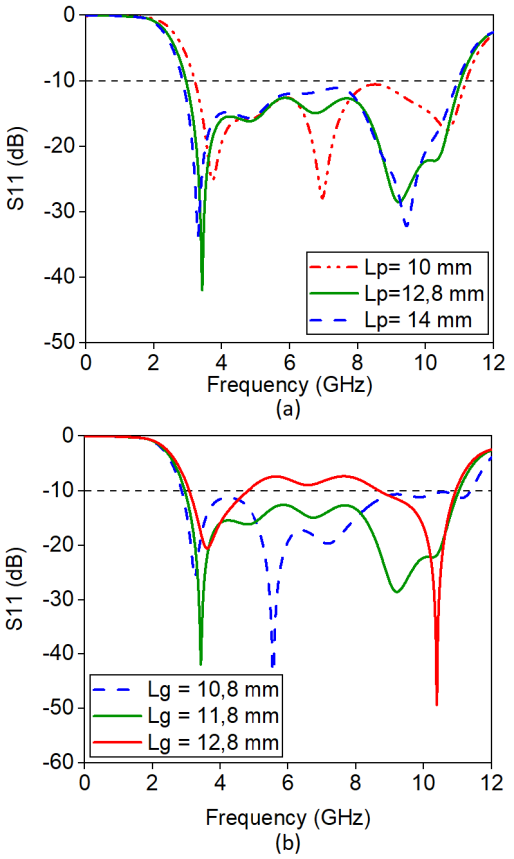

FIGURE 2. Effect of varying the lengths. (a) Length of the patch and, (b) length of the ground plane.

The fabricated UWB antenna is depicted in Fig. 1(b). Measurements are performed using the KEYSIGHT PNA N5224A network analyzer. Fig. 3 shows the measured and simulated magnitude of the reflection coefficient.

Based on [5], the dimension of T-shaped slots can be approximated by the following equation:

$$L_{tot} = L_t + W_t \approx \frac{\lambda_g}{4} \quad (1)$$

where λg is the guided wavelength of the newly created resonance at 9.2 GHz.

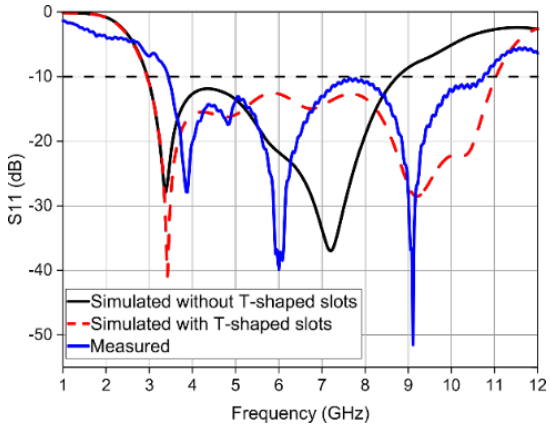

FIGURE 3. Magnitude of S_{11} for the designed UWB antenna.

The measurement setup for the radiation pattern of the proposed UWB antenna in the anechoic chamber is shown in Fig.4, the simulated and measured radiation patterns at both 4 GHz and 8 GHz are presented in Fig. 5. One can observe that the proposed antenna exhibits radiation patterns similar to those of a monopole antenna. It has an omnidirectional radiation pattern in the H-plane and a bi-directional radiation pattern in the E-plane.

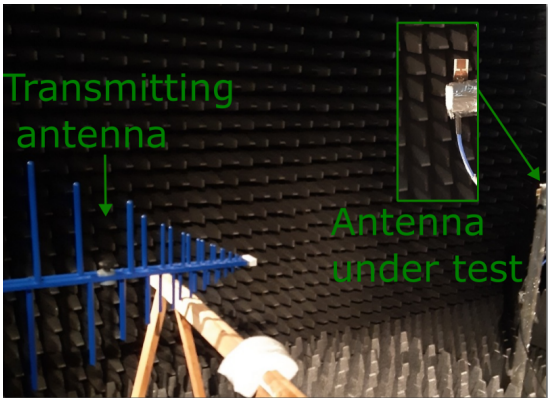

FIGURE 4. Measurement setup.

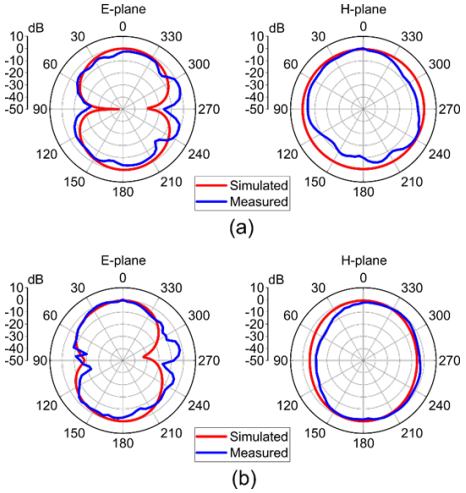

FIGURE 5. Radiation patterns at: (a) 4 GHz and, (b) 8 GHz

The input transmitted pulse (Tx) and the received one (Rx) for two identical antennas (face to face and side by side configurations) separated by a distance d of 150 mm are shown in Fig. 6. It can be seen that the shape of the pulse is conserved for both configurations.

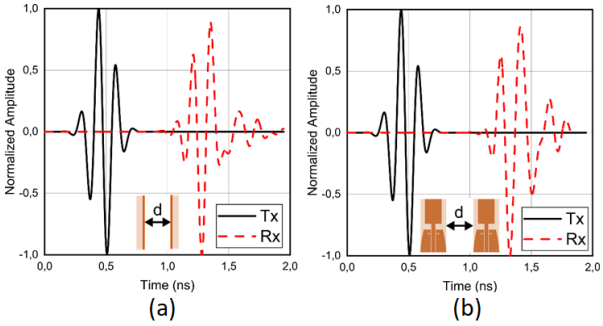

FIGURE 6. Transmitted and received pulses. (a) Face to face and, (b) Side by side.

B. FILTERING MECHANISM

To create a band-notch characteristic, an open loop resonator is inserted on the back face of the proposed UWB antenna (Fig. 7), close to the feedline and the radiating element, to enhance the coupling between the OLR and the antenna. The central frequency and filtering level of the band-notched depend on the OLR dimensions and its position. The considered dimensions of the OLR (placed at the position "O" with x=5.65 mm, y=11.8 mm), in order to obtain WLAN band-notch with a central frequency at 5.66 GHz, are: R=2.6 mm, W=0.6 mm, Gap=0.4 mm. Based on [24], the relationship between the central frequency of the band-notched and the OLR dimension is expressed by the following equation:

$$F_{notch} = \frac{C}{2L_{OLR}\sqrt{\varepsilon_{eff}}} \quad (2)$$

where

$$L_{OLR} = 2\pi R - Gap \quad (3)$$

$$\varepsilon_{eff} = \frac{\varepsilon_r + 1}{2} \quad (4)$$

C, ε_{eff} and L_{OLR} are speed of the light, effective permittivity, and total length of the OLR, respectively.

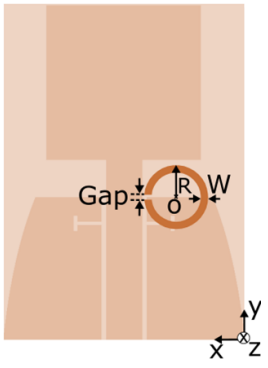

FIGURE 7. Geometry and position of the integrated OLR.

The equivalent circuit of the proposed UWB antenna with WLAN band-notched is shown in Fig. 8. It is approximated by using multiple cascaded LC resonator circuits [25]. The filtering effect generated by the OLR is represented by a parallel RnLnCn network [26].

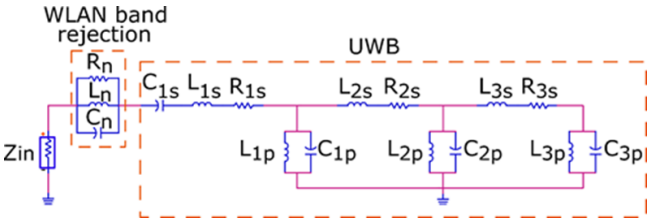

FIGURE 8. Equivalent circuit of the proposed UWB antenna with WLAN band-notched.

The considered values of the lumped elements are listed in Table II. The electromagnetic simulation, equivalent circuit simulation and measurement of S_{11} are shown in Fig. 9.

TABLE II. Optimized lumped elements values of the equivalent circuit

L	Value (nH)	C	Value (pF)	R	Value (ohm)
Ln	0.225	*Cn*	3.46	*Rn*	182
L1s	1.34	*C1s*	0.66	*R1s*	16.8
L2s	0.8	*C1p*	0.7	*R2s*	30
L3s	0.43	*C2p*	2	*R3s*	3.6
L1p	1.1	*C3p*	0.6		
L2p	2.13				
L3p	4.8				

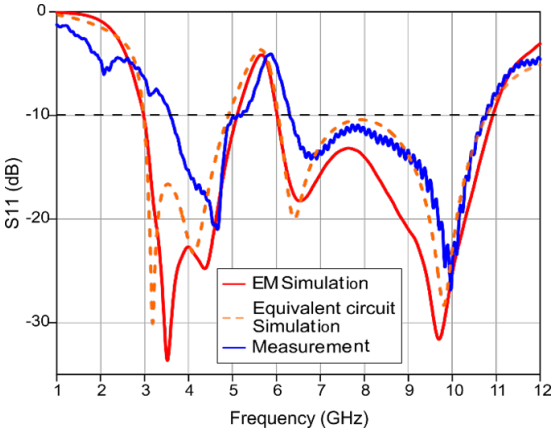

FIGURE 9. Magnitude of S_{11} for the proposed UWB antenna with WLAN band-notch characteristic.

Fig. 10 shows the surface current distribution at a frequency inside the rejected WLAN band (5.66 GHz), and at a frequency outside the WLAN band (8 GHz), respectively. The current is concentrated on the OLR at 5.66 GHz and is less dense at 8 GHz, which demonstrates the implication of the OLR on the WLAN band rejection. It captures frequencies proportional to its electrical length and lets the other frequencies pass to be radiated by the square patch.

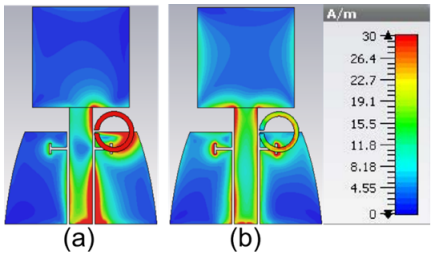

FIGURE 10. Simulated surface current distributions of the proposed antenna at: (a) 5.66 GHz and, (b) 8 GHz.

C. RECONFIGURATION MECHANISM

For the first phase of test and measurement, the switch states (ON/OFF) are modeled by the presence and absence of cooper (ideal switch). The optimal position to integrate the switch is in the middle of the OLR (Fig. 11(a)).

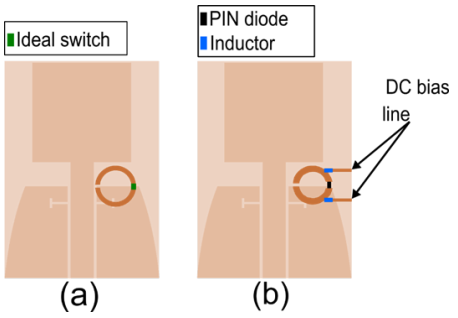

FIGURE 11. Reconfigurable antenna structure with. (a) Ideal switch and, (b) Real switch.

The surface current distribution at 5.66 GHz for both switch states is shown in Fig. 12, it demonstrates that when the switch is disabled, the current density is very low on the OLR, so the filter effect is disabled in this case and the UWB band is achieved without any frequency band rejection. When the switch is activated, an UWB antenna with WLAN band-notched is obtained (filter is enabled). The simulated and measured S_{11} of the two prototypes are presented in Fig. 13.

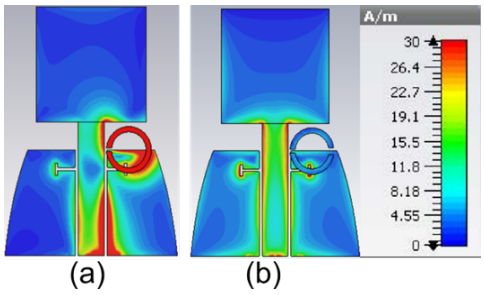

FIGURE 12. Simulated surface current distributions of the proposed antenna at 5.66 GHz. a Switch ON and, b Switch OFF.

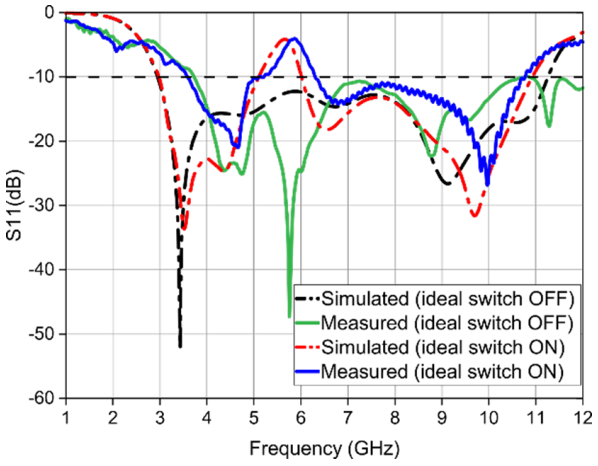

FIGURE 13. Magnitude of S_{11} for reconfigurable UWB antenna using ideal switch.

By comparing the realized gain as a function of frequency for the two modes illustrated in Fig. 14, it is observed that the gain drops significantly to the negative value at the notched WLAN band, regarding other operating frequencies the gain remains almost identical.

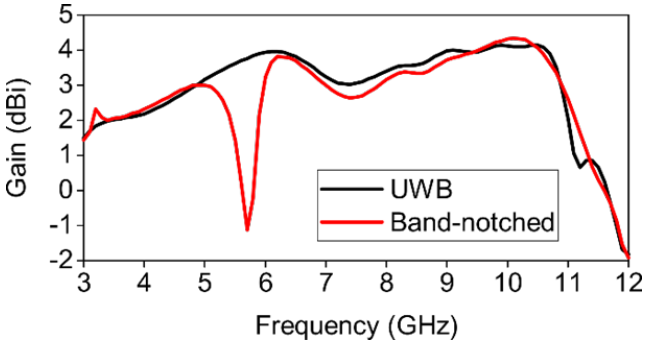

FIGURE 14. Realized gain of the reconfigurable antenna for both UWB and Band-notched modes.

For the final implementation with a real switch, a PIN diode SKYWORKS SMP1321-079LF up to 10 GHz, two inductors of 100 nH, which block the RF signal and allow the DC signal to pass through, and printed DC bias lines of 0.4 mm width are used (Fig. 11(b)). The PIN diode is simulated with the s2p file available on the manufacturer's website [27]. From the SMP1321 Series datasheet, at the ON state, the PIN diode is equivalent to a resistance Rs=2 Ω in series with parasitic inductance Ls=0.7 nH and, at the OFF state it is equivalent to a capacitor Ct=0.25 pF shunted by a parallel resistance Rp of high value similar to an open circuit in series with Ls. In the case of a real switch, some changes are made to the dimensions of the OLR (R=2.5 mm, W=0.8 mm) along with its position (x=3.75, y=12) in order to reduce the inductive and capacitive effects of the diode and remain centered on the notched WLAN band. The photograph of the fabricated reconfigurable antenna using a PIN diode is shown in Fig. 15, whereas Fig. 16 shows the simulated and measured S_{11}, the reconfiguration ability of the antenna is clearly seen, the slight variations in the measured results are primarily due to the impact of soldering the SMA connector to the feed line, and DC wires to DC bias lines.

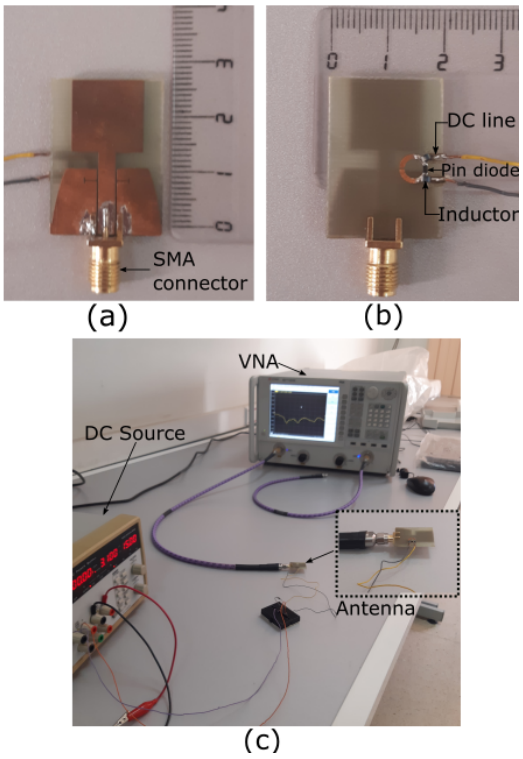

FIGURE 15. Photograph of the fabricated reconfigurable antenna. (a) Top view, (b) Bottom view, and (c) During measurement.

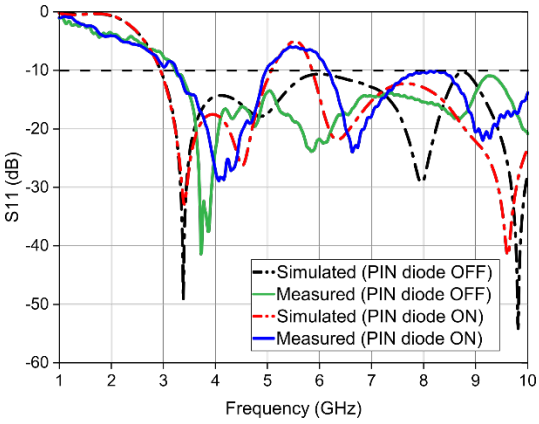

FIGURE 16. Magnitude of S_{11} for reconfigurable UWB antenna using a PIN diode.

III. BREAST TUMOR DETECTION

A hemispherical breast phantom is designed, with dimensions specified by a skin layer of 2 mm thickness, a fat layer of 48 mm thickness, and a spherical tumor with a radius of 5 mm lodged in the fat layer. The breast phantom is built using materials from the CST bio tissue library, except the tumor was created with a relative permittivity of 50, and 4 S/m of conductivity [7]. The dielectric properties of skin and fat are shown in Fig. 17.

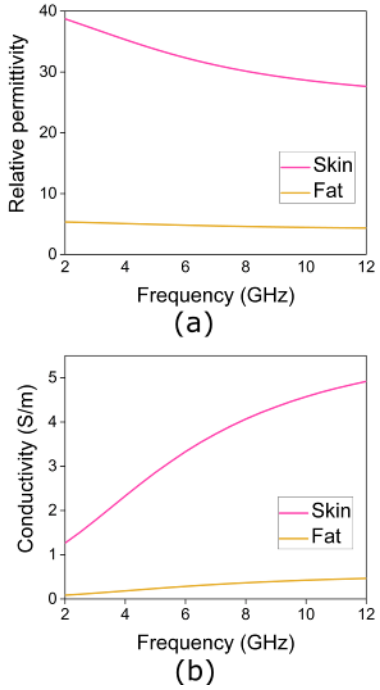

FIGURE 17. Dielectric properties of skin and fat layer. (a) Relative permittivity, and (b) Conductivity.

The antenna is set in a monostatic microwave imaging setup placed at 10 mm from the breast phantom, as presented in Fig. 18.

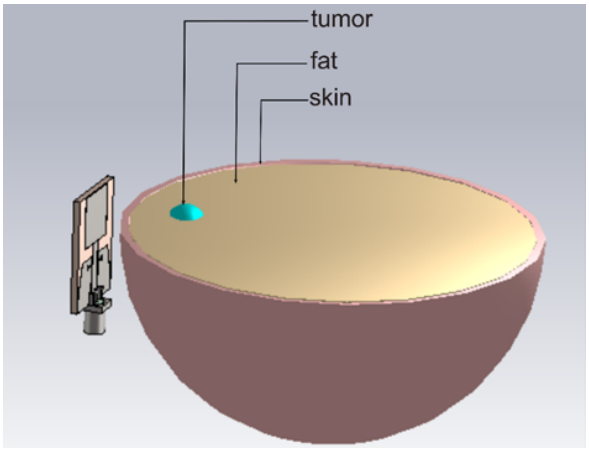

FIGURE 18. Simulation setup of the antenna and breast phantom.

Fig. 19 depicts the reflected signal in both the presence and absence of the tumor. It is noticeable that there is a contrast between the reflected signals, and that a signal indicating the existence of the tumor can be generated by subtracting the reflected signals (with tumor and without tumor). For the two operating modes of the antenna (UWB and band-notched UWB) it can be seen that the tumor detection is possible, which is a good solution for an interfered or an un-interfered environment.

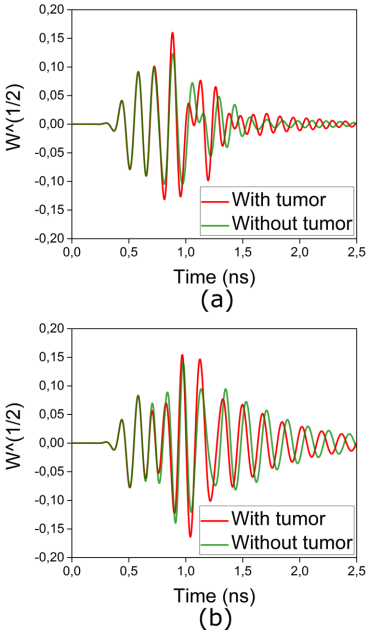

FIGURE 19. Reflected signal. (a) For UWB antenna mode and, (b) Band-notched UWB antenna mode.

Finally, a comparison in terms of bandwidth, peak gain, antenna size, and reconfigurability between the proposed antenna and some existing antennas for microwave imaging applications is illustrated in Table III.

TABLE III. Comparison between the proposed antenna and other previously published antennas

References	Size (mm^2)	Bandwidth (GHz)	Band-notched	Reconfigurability
[2]	*21 X 23*	3.1-12	without	No
[5]	12 X 18	2.96-15.8	without	No
[6]	64 X 63	2.89-12.58	without	No
[7]	30 X 30	3.04-19	without	No
[8]	31 X 31	3.04-11	without	No
[9]	33 X 14	3-11	without	No
[11]	67 X 46	4.6-8	without	No
[12]	45 X 40	2.79-16.66	without	No
[13]	15 X 18	4.11–29.77	X-band	No
[14]	20 X 28	3-13	WLAN, WiMAX	No
[15]	28X26	3.6-11	WLAN, WiMAX	No
[16]	58 X 27	3.1-10.6	WLAN	No
[22]	80 X 61	4-15	without	Yes
[23]	40 X 80	3.1-10	without	Yes
Current work	20 X 28	2.94-11	WLAN	Yes

IV. CONCLUSION

A compact and reconfigurable monopole antenna able to switch between UWB and WLAN band-notched modes is presented. The switching between the two modes is possible using a PIN diode inserted on an OLR. The simulated and measured results are in good agreement. The proposed antenna is suited to use for microwave imaging applications in the presence and/or absence of interferences.

REFERENCES

[1] M. Pastorino, "Applications of Microwave Imaging," in *Microwave Imaging*, Wiley, 2010.

[2] M. T. Islam, M. Samsuzzaman, M. N. Rahman, and M. T. Islam, "A compact slotted patch antenna for breast tumor detection," *Microw. Opt. Technol. Lett.*, vol. 60, no. 7, pp. 1600–1608, Jul. 2018.

[3] X. Li, E. J. Bond, B. D. Van Veen, and S. C. Hagness, "An overview of ultra-wideband microwave imaging via space-time beamforming for early-stage breast-cancer detection," *IEEE Antennas Propag Mag*, vol. 47, no. 1, pp. 19–34, Jan. 2005.

[4] D. Bhargava, P. Rattanadecho, and K. Jiamjiroch, "Microwave Imaging for Breast Cancer Detection - A Comprehensive Review," Engineered Science, 2024.

[5] A. Abdollahvand, A. Pirhadi, H. Ebrahimian, and M. Abdollahvand, "A compact UWB printed antenna with bandwidth enhancement for in-body microwave imaging applications," *Prog. Electromagn. Res. C.*, vol. 55, pp. 149-157, 2014.

[6] I. Hossain, S. Noghanian, L. Shafai, and S. Pistorius, "Coplanar waveguide fed taper arc slot antenna for microwave imaging and ultra-wide band applications," *Microw. Opt. Technol. Lett.*, vol. 51, no. 11, pp. 2607-2611, Nov. 2009.

[7] H. Li, H. Zhang, Y. Kong, and C. Zhou, "Flexible Dual-Polarized UWB Antenna Sensors for Breast Tumor Detection," *IEEE Sens. J.*, vol. 22, no. 13, pp. 13648-13658, Jul. 2022.

[8] M. Z. Mahmud, M. T. Islam, and M. Samsuzzaman, "A high-performance UWB antenna design for microwave imaging system," *Microw. Opt. Technol. Lett.*, vol. 58, no. 8, pp. 1824-1831, Aug. 2016.

[9] I. M. Danjuma, M. O. Akinsolu, C. H. See, R. A. Abd-Alhameed, and B. Liu, "Design and optimization of a slotted monopole antenna for ultra-wide band body-centric imaging applications," *IEEE J. Electromagn. RF Microw. Med.*, vol. 4, no. 2, pp. 140-147, Apr. 2020.

[10] O. P. Kumar, T. Ali, and P. Kumar, "A Novel Corner Etched Rectangular shaped Ultrawideband Antenna Loaded with Truncated Ground Plane for Microwave Imaging," *Wirel. Pers. Commun.*, vol. 130, no. 3, pp. 2241-2259, Mar. 2023.

[11] M. Slimi, B. Jmai, H. Dinis, A. Gharsallah, and P. M. Mendes, "Metamaterial vivaldi antenna array for breast cancer detection," *Sensors*, vol. 22, no. 10, pp. 3945, May 2022.

[12] S. Sasikala, K. Karthika, S. Arunkumar, K. Anusha, S. Adithya, and A. J. A. Al-Gburi, "Design and Analysis of a Low-Profile Tapered Slot UWB Vivaldi Antenna for Breast Cancer Diagnosis," *Prog. Electromagn. Res. M.*, vol. 124, pp. 43-51, 2024.

[13] V. P. Ponnapalli, S. Karthikeyan, J. Lakshmi Narayana, and V. K. Devana, "A compact SE-DGS tapered-fed notched UWB antenna integrated with Ku/K band for breast cancer detection," *IETE J. Res.*, pp. 1-11, 2023.

[14] A. Kaabal, S. Ahyoud, and A. Asselman, "Dual Band-Notched WIMAX/WLAN of a Compact Ultrawideband Antenna with Spectral and Time Domains Analysis for Breast Cancer Detection," *Prog. Electromagn. Res. C.*, vol. 65, 2016.

[15] I. Amdaouch, O. Aghzout, A. Naghar, A. V. Alejos, and F. Falcone, "Enhanced Accuracy of Breast Cancer Detection Based on UWB Compact Slotted Monopole Antennas," *Advanced Electromagnetics*, vol. 8, no. 5, pp. 1-6, 2019.

[16] F. Latif, F. A. Tahir, M. U. Khan, and M. S. Sharawi, "An ultra-wideband diversity antenna with band-rejection capability for imaging applications," *Microw. Opt. Technol. Lett.*, vol. 59, no. 7, pp. 1661-1668, Jul. 2017.

[17] S. Goel and N. Gupta, "Design, optimization and analysis of reconfigurable antenna using RF MEMS switch," *Microsyst. Technol.*, vol. 26, pp. 2829-2837, 2020.

[18] V. M. Lad, K. V. Kulhalli, J. Kumar, and G. Patil, "Frequency-Tunable Multiband Reconfigurable Microstrip Patch Antenna for Wireless Application," *Wirel. Pers. Commun.*, vol. 130, no. 2, pp. 1231-1242, Feb. 2023.

[19] M. Bitchikh, M. Mokhtari, and W. Rili, "Switchable UWB/narrowband/bi-bands octagonal antenna using PIN diodes," *Electron. Lett.*, vol. 54, no. 8, pp. 480-482, Apr. 2018.

[20] S. Mudda, K. M. Gayathri, and M. Mallikarjun, "Efficient Frequency Reconfigurable Antenna for 4G, Sub-6 GHz, 5G Portable Devices Applications," *Wirel. Pers. Commun.*, vol. 129, no. 4, pp. 2711-2725, Apr. 2023.

[21] A. Mansoul, F. Ghanem, M. R. Hamid, and M. Trabelsi, "A selective frequency-reconfigurable antenna for cognitive radio applications," *IEEE Antennas Wirel. Propag. Lett.*, vol. 13, pp. 515-518, 2014.

[22] K. Hossain, T. Sabapathy, M. Jusoh, S. H. Lee, K. S. A. Rahman, and M. R. Kamarudin, "Negative index metamaterial-based frequency-reconfigurable textile CPW antenna for microwave imaging of breast cancer," *Sensors*, vol. 22, no. 4, pp. 1626, Feb. 2022.

[23] S. Lim, and Y. J. Yoon, "Wideband-narrowband switchable tapered slot antenna for breast cancer diagnosis and treatment," *Appl. Sci.*, vol. 11, no. 8, pp. 3606, Feb. 2021.

[24] Q. X. Chu, and Y. Y. Yang, "A compact ultrawideband antenna with 3.4/5.5 GHz dual band-notched characteristics," *IEEE Trans. Antennas Propag.*, vol. 56, no. 12, pp. 3637-3644, Dec. 2008.

[25] M. N. Hasan, S. Chu, and S. Bashir, "A DGS monopole antenna loaded with U-shape stub for UWB MIMO applications," *Microw. Opt. Technol. Lett.*, vol. 61, no. 9, pp. 2141-2149, Sep. 2019.

[26] B. Biswas, R. Ghatak, A. Karmakar, and D. Poddar, "Dual band notched UWB monopole antenna using embedded omega slot and fractal shaped ground plane," *Prog. Electromagn. Res. C.*, vol. 53, pp. 177-186, 2014.

[27] Skyworks, "Products details," [Online]. Available: https://www.skyworksinc.com/en/products/diodes/smp1321%20series/, Accessed on: Feb.19, 2024.